Applied Physics Letters

Enhancement of graphene-related and substrate-related Raman modes through dielectric layer deposition

Cite as: Appl. Phys. Lett. **120**, 063105 (2022); https://doi.org/10.1063/5.0082694
Submitted: 17 December 2021 • Accepted: 28 January 2022 • Published Online: 09 February 2022

Karolina Piętak, Jakub Jagiełło, Artur Dobrowolski, et al.

Applied Physics Letters ARTICLE scitation.org/journal/apl

Enhancement of graphene-related and substrate-related Raman modes through dielectric layer deposition

Cite as: Appl. Phys. Lett. **120**, 063105 (2022); doi: 10.1063/5.0082694
Submitted: 17 December 2021 · Accepted: 28 January 2022 ·
Published Online: 9 February 2022

Karolina Piętak,[1,2,3,a)] Jakub Jagiełło,[1,4] Artur Dobrowolski,[1,4] Rafał Budzich,[1,2,3] Andrzej Wysmołek,[4] and Tymoteusz Ciuk[1]

AFFILIATIONS

[1]Łukasiewicz Research Network-Institute of Microelectronics and Photonics, Al. Lotników 32/46, 02-668 Warsaw, Poland
[2]Faculty of Chemistry, Warsaw University of Technology, ul. Noakowskiego 3, 00-664 Warsaw, Poland
[3]Warsaw University of Technology, Doctoral School No 1, ul. Plac Politechniki 1, 00-661 Warsaw, Poland
[4]Faculty of Physics, University of Warsaw, ul. Pasteura 5, 02-093 Warsaw, Poland

[a)]**Author to whom correspondence should be addressed:** karolina.pietak@imif.lukasiewicz.gov.pl

ABSTRACT

In this report, we demonstrate a method for the enhancement of Raman active modes of hydrogen-intercalated quasi-free-standing epitaxial chemical vapor deposition graphene and the underlying semi-insulating 6H–SiC(0001) substrate through constructive signal interference within atomic-layer-deposited amorphous Al_2O_3 passivation. We find that an optimum Al_2O_3 thickness of 85 nm for the graphene 2D mode and one of 82 nm for the SiC longitudinal optical A_1 mode at 964 cm^{-1} enable a 60% increase in their spectra intensities. We demonstrate the method's efficiency in Raman-based determination of the dielectric thickness and high-resolution topographic imaging of a graphene surface.

Although intensively researched since the 2004 original work of Novoselov,[1] graphene remains an attractive two-dimensional (2D) material for Raman study. However, due to its one-atom-thick structure, it transmits much of the incident light,[2] generating only a small portion of scattered radiation.[3] Moreover, the reduced intensity of graphene spectra hinders the determination of its subtle characteristics, including vacancies, edge structure, doping type and level, attached functional groups, and crumpling.[3,4]

Enhancement of the Raman signal intensity is currently among the most researched directions in developing Raman-based characterization techniques of all 2D materials as it elevates detection limits of their fine structural properties. The interest in Raman signal intensification is also triggered by the wide range of applications it can benefit. These include biochemistry and biosensing,[5–7] polymer and materials science,[8–11] catalysis,[12,13] electrochemistry,[7,14] the study of high-temperature processes,[15] and detection of hazardous gases.[7,16]

Traditionally, the Raman signal is intensified by either *surface*-enhancement[17] (SERS) or *interference*-enhancement (IERS). The first technique takes advantage of plasmonic effects occurring on the surface of nanostructured metallic particles placed onto the studied material.[18] The latter method was first described by Connell in 1980.[9] It assumes that the effective reflection of a coherent signal from a stack of dielectric layers is limited by wave interference, which leads to the signal's amplification or extinction. In a system of a beam traveling through the air and reaching the surface of a stack of two dielectric layers, of which the top one is described by a refractive index n_1 and the bottom one by n_2, the condition for wave enhancement assumes that the optical thickness of the top layer d_1n_1, d_1 being the top layer's physical thickness, is given by

$$2d_1n_1 = \left(m + \frac{1}{2}\right)\lambda, \quad m = 0, 1, 2, \ldots, \tag{1}$$

where m is a natural number, $\frac{1}{2}$ describes phase shift by π for $n_2 > n_1$, and λ is the signal's wavelength.

The material under study may be placed *on top* of a two-layer system comprising a phase-shifting dielectric on a light-reflecting substrate.[3,10,19] It has been found by Gao *et al.* that graphene modes are significantly amplified when it rests on a 70-nm-thick Al_2O_3 layer on a silicon substrate.[3] In addition to aluminum oxide, SiO_2,[11] TiO_2,[20] or one-dimensional photonic crystals[21] can be used as phase-shifting

layers. What remains essential for IERS is the number of the graphene layers as it was proven by Wang *et al.* that in a stack of ten or more of them on SiO_2, the Raman signal is intensified by light multi reflections from the individual sheets.[11]

This research presents an interesting approach to the interference-enhancement of graphene-related and substrate-related Raman active modes in a system comprising graphene sandwiched between two dielectric layers. The top-most layer is atomic-layer-deposited (ALD) amorphous Al_2O_3, and the bottom one is semi-insulating monocrystalline SiC(0001), as it is the primary structure suggested for the environmentally protected high-temperature Hall effect sensors.[22,23]

We exploit a model proposed by Vanco *et al.*,[24] which describes Raman signal amplification through an enhancement factor (EF). The model is adapted for the Al_2O_3/graphene/SiC system and a reference one of Al_2O_3 on silicon. With the Al_2O_3 layer thickness spanning the range between 0 and 180 nm, we plot theoretical lines of the EF determined for the SiC longitudinal optical (LO) A_1 mode at 964 cm^{-1} and the Si-related mode at 520 cm^{-1} and confront them with the EF's experimental values to find significant correspondence. The experimental verification is further enriched with graphene G and 2D modes that prove most pronounced at a specific passivation thickness.

Finally, upon the analysis of the theoretical and experimental EF related to the Al_2O_3 thickness and supported by spectroscopic ellipsometry, we consider two practical applications of *passivation*-enhanced Raman spectroscopy—improved topographic imaging of the graphene surface and Raman-based assessment of the dielectric thickness.

Quasi-free-standing (QFS) graphene[25,26] was grown on a semi-insulating vanadium-compensated on-axis 20×20 mm^2 6H–SiC(0001) substrate (II-VI, Inc.) through epitaxial chemical vapor deposition (CVD) followed by *in situ* hydrogen-intercalation[27] in the hot-wall Epigress VP508 reactor.[28] Propane was used as a carbon source. Then the substrate was diced into several 5×5 mm^2 individual samples to guarantee possibly high uniformity of graphene and the substrate properties.

Amorphous Al_2O_3 was applied onto the 5×5 mm^2 QFS graphene on SiC samples by atomic layer deposition (ALD) in a 4-in Picosun R200 advanced at 300 °C. Trimethylaluminum (TMA) and de-ionized water (DI) were used as the source of aluminum and oxygen, respectively. A reference silicon sample (with the native oxide pre-removed with water-diluted hydrofluoric acid) was added to each process. The deposition procedure consisted of an annealing step at 300 °C followed by 250–1250 cycles (500–2500 half-cycles of DI and TMA) at the same temperature. Following the threshold of 40 cycles suggested by Schilirò *et al.* for non-intercalated *n*-type graphene,[29,30] the minimum number of 250 cycles was expected to guarantee full and homogeneous coverage, even though the *p*-type conductance only limited the already hindered nucleation of Al_2O_3.

The reference silicon samples present in the ALD processes were used to verify the physical thickness of the deposited Al_2O_3 layers using the EP4SE Accurion spectral imaging ellipsometer. It was assumed that the graphene on SiC samples shared identical passivation thickness and, therefore, was not verified. The measurements were carried out in a nulling regime for the spectral range of 300–500 nm with a step of 5 nm and an angle of incidence (AOI) equals 50°. A Nanochromat NC2 UV-VIS-NIR microscope objective with a field of view (FOV) of 0.78 mm was used for the measurement. The physical thickness of the Al_2O_3 layers was derived from an Accurion predefined model for amorphous aluminum oxide.

Single Raman spectra of graphene, the underlying silicon carbide,[31] and the reference silicon substrates were obtained in a back-scattering geometry of the Renishaw inVia confocal microscope using the 532-nm (2.33 eV) line of a continuous-wave Nd:YAG laser and the Andor Newton CCD detector. A 5× objective with a numerical aperture (NA) of 0.25 was chosen for the Si-related mode 520 cm^{-1} in full accordance with the Vanco *et al.* publication. In the case of the faint signal of epitaxial graphene on SiC, we were forced to use a 100× objective with NA = 0.95 to be able to extract meaningful data. Following this restriction, we used the same conditions (100× objective) to visualize the SiC-related longitudinal optical (LO) A_1 mode at 964 cm^{-1} only to be able to directly compare both images. The laser power was kept at 100% (13.5 mW) throughout the experiment. The signals of the SiC-related and the Si-related modes were recorded in the near-surface region and averaged five times to improve their readability.

A 4624-point 20×20 μm^2 map imaging graphene on SiC was measured with a lateral step of 0.3 μm in both the *X* and *Y* directions. It spanned the spectra from 1300 to 2830 cm^{-1} and was repeated 4 μm below the SiC(0001) surface to provide reference for the graphene modes fitted with a mixture of Gaussian and Lorentzian line shapes.

In order to plot the theoretical EF curves as a function of the Al_2O_3 thickness ranging from 0 to 180 nm based on the model adapted from Vanco *et al.*, it was assumed that graphene has a negligible volumetric contribution to the dielectric stack, and therefore, its optical properties may be ignored in the theoretical model. What was accounted for were the wavelengths of the incident laser line (532 nm) and the back-scattered signals bearing in mind that the Si-related Raman mode at 520 cm^{-1} corresponds to a Stokes line of 547 nm, the SiC-related Raman mode at 964 cm^{-1} to a Stokes line of 561 nm, and the graphene 2D mode at 2708 cm^{-1} to 621 nm.

Refractive indices necessary to calculate the amplitude reflection coefficients $r_{ij} = \frac{n_i - n_j}{n_i + n_j}$, where n is the refractive index and i, j label the different materials,[24] were copied from models for crystalline silicon carbide and crystal silicon delivered by the EP4SE Accurion library and summarized in Table I.

Schematics of the two considered systems: Al_2O_3-passivated QFS graphene on 6H–SiC(0001) and the reference Al_2O_3-passivated silicon are shown in Fig. 1.

TABLE I. Refractive indices and amplitude reflection coefficients used to calculate theoretical EFs at wavelengths of the incident light and the scattered Stokes lines.

	Laser 532 nm	Si 547 nm	SiC 561 nm	GR 621 nm
n_1 (Air)	1.000	1.000	1.000	1.000
n_2 (Al_2O_3)	1.664	1.663	1.662	1.659
n_3 (SiC)	2.713	×	2.699	2.678
n_3 (Si)	4.152	4.096	×	×
r_{12}	−0.249 25	−0.248 97	−0.248 69	−0.247 84
r_{23} (SiC)	−0.239 66	×	−0.237 79	−0.234 96
r_{23} (Si)	−0.427 79	−0.422 47	×	×

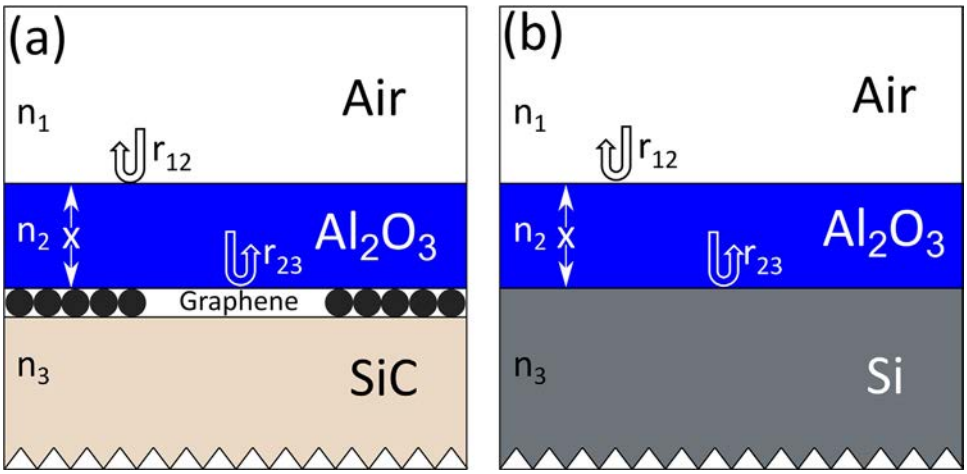

FIG. 1. Schematic of the two considered systems. (a) Amorphous atomic-layer-deposited Al_2O_3 on hydrogen-intercalated QFS epitaxial CVD graphene on semi-insulating vanadium-compensated on-axis 6H–SiC(0001). (b) Amorphous atomic-layer-deposited Al_2O_3 on reference monocrystalline silicon.

The comparison of the theoretical EF with the experimentally found values for the two considered systems from Fig. 1 is presented in Fig. 2. It is evident that the EF measured for the SiC LO A_1 mode at 964 cm^{-1} (marked in beige), the Si mode at 520 cm^{-1} (marked in gray), and the graphene 2D mode at 621 cm^{-1} (marked in black) correlate with the theoretical predictions.

The enhancement factor for the SiC mode at 964 cm^{-1} reaches its highest value $EF = 1.60$ for the Al_2O_3 thickness $d = 82$ nm. In the case of the Si mode at 520 cm^{-1}, the highest value of $EF = 2.33$ occurs at $d = 81$ nm. Since the wavelength of the scattered signal associated with the graphene 2D band is slightly longer, the corresponding EF equals 1.59 at $d = 85$ nm. In all cases, the optimum passivation thickness is consistent with the quarter-wavelength of the incident 532-nm laser line in amorphous aluminum oxide.

As the wavelength of the scattered light associated with the graphene G band at 1590 cm^{-1} is 40 nm shorter than the one of the 2D band, the theoretical EF curve for the former is expected to lie between the one for the SiC LO and the graphene 2D. The effect of signal enhancement on the individual Raman spectra of QFS graphene on SiC is illustrated in Fig. 3.

Spectroscopic ellipsometry is a valuable method for determining the thickness of a dielectric and its refractive index. However, fitting experimental data points to spectroscopic models may prove demanding in complex multi-layer structures. Here, we propose an alternative

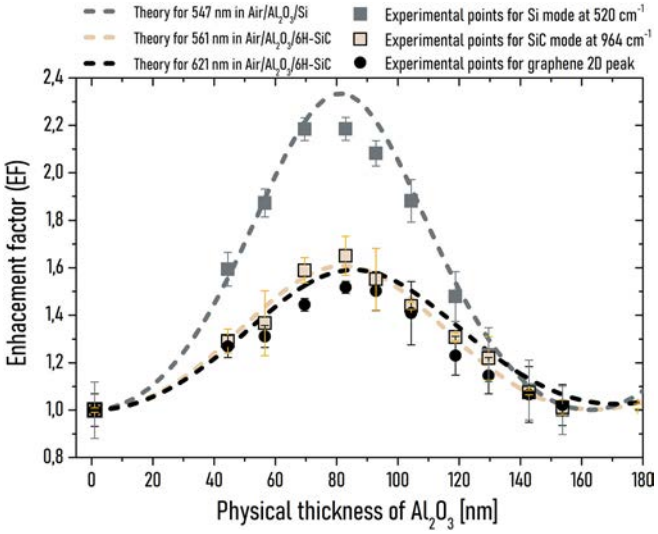

FIG. 2. Theoretical (dashed lines) and experimental (square symbols) enhancement factor (EF) for the SiC LO A_1 mode at 964 cm^{-1} (marked in beige), the Si mode at 520 cm^{-1} (marked in gray), and the QFS graphene 2D mode at 2708 cm^{-1} (marked in black), all as a function of the Al_2O_3 physical thickness. The error bars come as standard deviations (1σ) of the measured EFs.

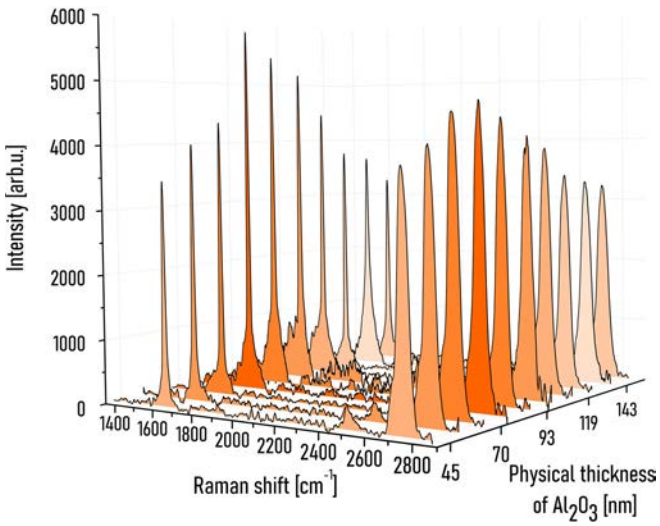

FIG. 3. Individual Raman spectra of hydrogen-intercalated QFS epitaxial CVD graphene on semi-insulating vanadium-compensated on-axis 6H–SiC(0001) as intensified by the varying thickness of the atomic-layer-deposited Al_2O_3 in the range between 45 and 154 nm. The figure corresponds to Fig. 2. The colors of the individual spectra reflect gradual change in the signal intensity.

method for calculating the passivation thickness. The method draws from the above-described changes of the EF of the substrate-related Raman active modes and the theoretical curves serving as a calibration standard.

If one treated the dashed gray line from Fig. 2 as a calibration curve for Al_2O_3 layers on silicon then knowing the experimental EF of the substrate-related mode at 520 cm^{-1}, they could assess the dielectric thickness. A good comparison of Raman-based and ellipsometric verification of the Al_2O_3/Si samples as a function of the number of the ALD cycles is presented in Fig. 4. The comparative ellipsometric assessment was provided through the Accurion model for amorphous aluminum oxide.

It can be concluded that within a measurement error of 5% or less, it is possible to determine the Al_2O_3 thickness. There is an inherent disadvantage of the technique resulting from the theoretical EF curve's cyclic character that ascribes multiple values of the dielectric thickness to a single EF, hence the two possible datasets for the Raman-derived thickness [green squares in Fig. 4(c)]. With little additional knowledge of the material under study, one may deduce the correct value from two possibilities. In this experiment, the correct dataset in Fig. 4(c) is the ascending one (surrounded by an ellipse). Still, bearing in mind the micro-Raman setup's potential for high-resolution mapping in X and Y directions, the Raman-based verification offers the possibility for precise thickness mapping.

Another possible use of signal interference amplification is the improvement of micro-Raman topographic imaging. As previously evidenced in Fig. 2, a 69-nm Al_2O_3 passivation provides a 44% higher intensity of the graphene modes. Therefore, one should expect improvement in the quality of *intensity-dependent* topographic imaging based on the SiC substrate response[31] over imaging that is *intensity-independent*, which holds for the 2D band's FWHM (full width at half-maximum). Figure 5 illustrates the 4624-point $20 \times 20\ \mu m^2$ Raman map of a QFS graphene on the SiC sample passivated with a 69-nm layer of Al_2O_3. The map exposes five terraces and four-step

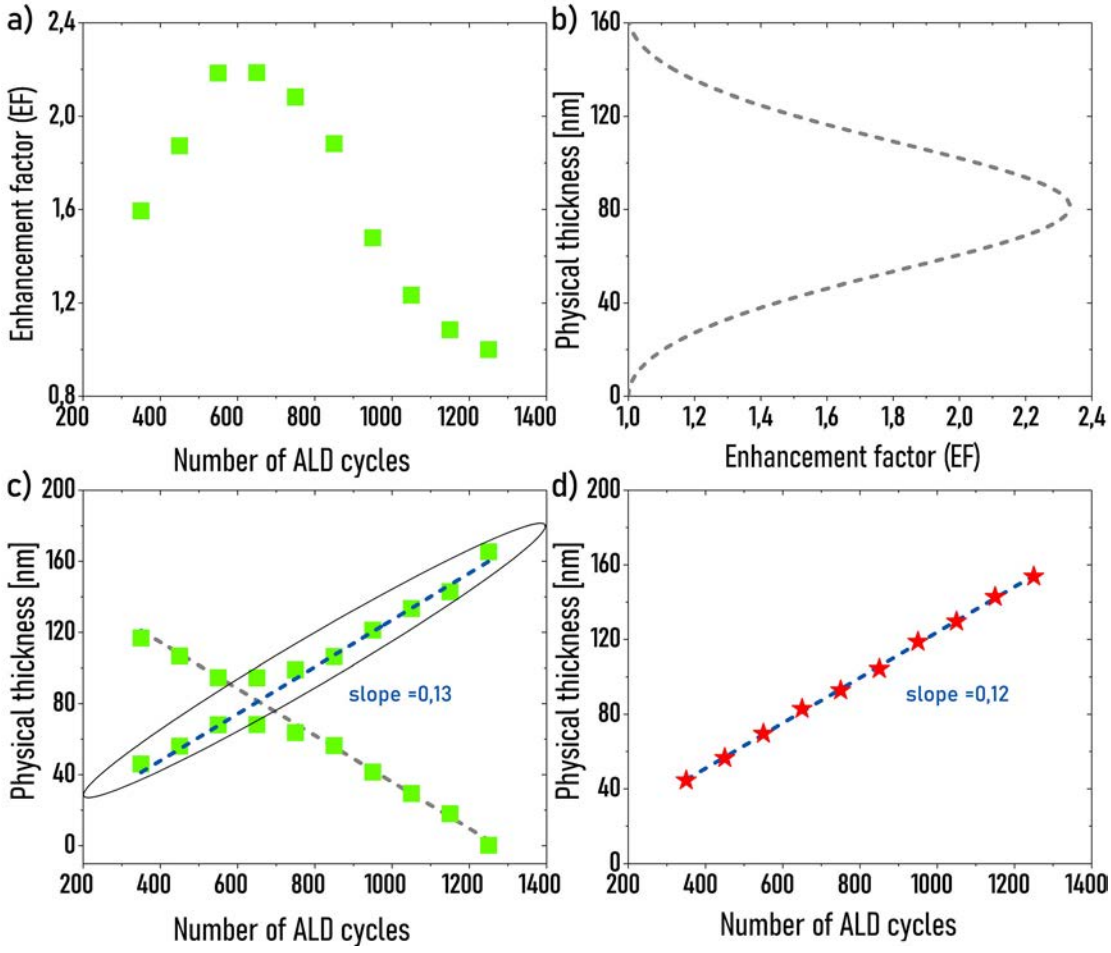

FIG. 4. Comparison of Raman-based (green squares) and ellipsometric (red stars) verification of the thickness of atomic-layer-deposited (ALD) Al_2O_3 on silicon. (a) Experimental enhancement factor (EF) for the Si mode at 520 cm^{-1} as a function of the number of the ALD cycles. (b) Physical Al_2O_3 thickness as a function of the EF. (c) Physical Al_2O_3 thickness derived from (a) and (b). (d) Physical Al_2O_3 thickness derived from spectroscopic ellipsometry. The slopes refer to the regression lines best fitting the data points.

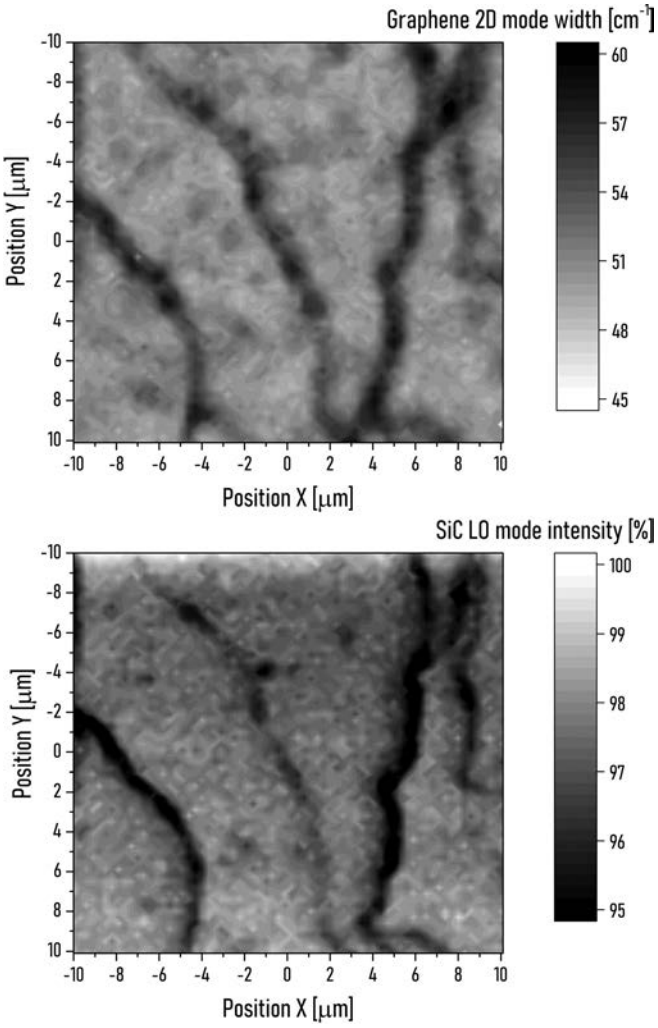

FIG. 5. High-resolution Raman map of hydrogen-intercalated QFS epitaxial CVD graphene on semi-insulating vanadium-compensated on-axis 6H–SiC(0001) passivated with 69-nm-thick atomic-layer-deposited Al_2O_3. (a) Graphene 2D mode FWHM. (b) Relative intensity of the SiC longitudinal optical A_1 mode at 964 cm^{-1}.

edges covered with additional elongated graphene domains, imaged in two alternative ways.

In this particular sample, the terraces appear to be decorated with a QFS monolayer^{plus}—a QFS monolayer with some statistical share of a QFS bilayer, and the step edges appear to be decorated with a QFS bilayer^{mixed}—a QFS bilayer with some statistical share of a QFS monolayer and some statistical share of a QFS trilayer, following the original methodology published in Ref. 31. However, since in this experiment, no *mesa*-like structure was fabricated, and therefore, no reference graphene-free region was available to serve as a normalization factor for the 964 cm^{-1} mode intensity, the protocol of Ref. 31 could not be fully exploited.

Also, the I_{2D}/I_G-based verification of the number of the graphene layers could not be directly applied as the Stokes lines associated with these modes differ in their wavelength. The 2D mode at 2708 cm^{-1} corresponds 621 nm while the G mode at 1590 cm^{-1} to 582 nm; therefore, for a given Al_2O_3 thickness, they experience different enhancement factors.

The remaining approach judges the number of layers by the 2D band FWHM. As illustrated in Fig. 5(a) within the terraces, the 2D band FWHM is ∼48–53 cm^{-1} (an expected value of 50.6 cm^{-1}) and broadens to ∼48–58 cm^{-1} (an expected value of 53.2 cm^{-1}) at the step edges. By common definition, the terraces would be categorized as containing both a QFS monolayer and a QFS bilayer and the step edges as a likely QFS trilayer.

Regardless of the structural quality of graphene, it is apparent that the intensity-dependent SiC LO mode intensity map is of higher resolution and contains more topographic details than the map of the intensity-independent 2D bandwidth.

In this report, we have shown that it is possible to enhance Raman signals of both hydrogen-intercalated QFS graphene and the underlying semi-insulating vanadium-compensated on-axis 6H–SiC(0001) substrate through constructive signal interference within the applied dielectric passivation, in this case, atomic-layer-deposited amorphous Al_2O_3.

It was found that an optimum passivation thickness that enables the highest enhancement factor is a quarter-wavelength of the incident laser line in Al_2O_3, only slightly enlarged due to Raman shift of the back-scattered light. As a result, it is 81 nm for the Si mode at 520 cm^{-1}, 82 nm for the SiC mode at 964 cm^{-1}, and 85 nm for the graphene 2D mode.

Two practical applications of passivation-enhanced Raman spectroscopy were demonstrated: first, as a tool for the thickness determination of the deposited Al_2O_3, fully compliant with ellipsometric verification, and second, as a resolution intensifier applicable to the technique of graphene topographic imaging through Raman response of the substrate.

The research leading to these results has received funding from the Research Foundation Flanders (FWO) under Grant No. EOS 30467715, the National Science Centre under Grant Agreement No. OPUS 2019/33/B/ST3/02677 for project "Influence of the silicon carbide and the dielectric passivation defect structure on high-temperature electrical properties of epitaxial graphene," and the National Centre for Research and Development under Grant Agreement No. LIDER 0168/L-8/2016 for the project "Graphene on silicon carbide devices for magnetic field detection in extreme temperature conditions."

Karolina Piętak and Rafał Budzich acknowledge financial support from the IDUB project (Scholarship Plus programme).

AUTHOR DECLARATIONS

Conflict of Interest

The authors have no conflicts to disclose.

DATA AVAILABILITY

The data that support the findings of this study are available from the corresponding author upon reasonable request.

REFERENCES

[1]K. S. Novoselov, "Electric field effect in atomically thin carbon films," Science **306**, 666–669 (2004).

[2]R. R. Nair, P. Blake, A. N. Grigorenko, K. S. Novoselov, T. J. Booth, T. Stauber, N. M. R. Peres, and A. K. Geim, "Fine structure constant defines visual transparency of graphene," Science **320**, 1308–1308 (2008).
[3]L. Gao, W. Ren, B. Liu, R. Saito, Z.-S. Wu, S. Li, C. Jiang, F. Li, and H.-M. Cheng, "Surface and interference coenhanced Raman scattering of graphene," ACS Nano **3**, 933–939 (2009).
[4]J. Niu, V. G. Truong, H. Huang, S. Tripathy, C. Qiu, A. T. S. Wee, T. Yu, and H. Yang, "Study of electromagnetic enhancement for surface enhanced Raman spectroscopy of SiC graphene," Appl. Phys. Lett. **100**, 191601 (2012).
[5]A. El-Ansary and L. Faddah, "Nanoparticles as biochemical sensors," Nanotechnol., Sci. Appl. **3**, 65–76 (2010).
[6]S. Pahlow, T. Mayerhöfer, M. van der Loh, U. Hübner, J. Dellith, K. Weber, and J. Popp, "Interference-enhanced Raman spectroscopy as a promising tool for the detection of biomolecules on Raman-compatible surfaces," Anal. Chem. **90**, 9025–9032 (2018).
[7]B. Sharma, R. R. Frontiera, A.-I. Henry, E. Ringe, and R. P. Van Duyne, "SERS: Materials, applications, and the future," Mater. Today **15**(1–2), 16–25 (2012).
[8]S. Fateixa, H. I. Nogueira, and T. Trindade, "SERS research applied to polymer based nanocomposites," in *Raman Spectroscopy* (InTech, 2018).
[9]G. A. N. Connell, R. J. Nemanich, and C. C. Tsai, "Interference enhanced Raman scattering from very thin absorbing films," Appl. Phys. Lett. **36**, 31–33 (1980).
[10]S. Kanakaraju, A. Sood, and S. Mohan, "Interference enhanced Raman spectroscopy of ultra thin crystalline Ge films," Curr. Sci. **74**, 322–327 (1998).
[11]Y. Y. Wang, Z. H. Ni, Z. X. Shen, H. M. Wang, and Y. H. Wu, "Interference enhancement of Raman signal of graphene," Appl. Phys. Lett. **92**, 043121 (2008).
[12]K. N. Heck, B. G. Janesko, G. E. Scuseria, N. J. Halas, and M. S. Wong, "Observing metal-catalyzed chemical reactions in situ using surface-enhanced Raman spectroscopy on Pd-Au nanoshells," J. Am. Chem. Soc. **130**, 16592–16600 (2008).
[13]A. V. Whitney, J. W. Elam, P. C. Stair, and R. P. V. Duyne, "Toward a thermally robust operando surface-enhanced Raman spectroscopy substrate," J. Phys. Chem. C **111**, 16827–16832 (2007).
[14]W. Paxton, S. Kleinman, A. Basuray, J. Stoddart, and R. Van Duyne, "Surface-enhanced Raman spectroelectrochemistry of TTF-modified self-assembled monolayers," J. Phys. Chem. Lett. **2**, 1145–1149 (2011).
[15]X. Li, J.-P. Lee, K. S. Blinn, D. Chen, S. Yoo, B. Kang, L. A. Bottomley, M. A. El-Sayed, S. Park, and M. Liu, "High-temperature surface enhanced Raman spectroscopy for *in situ* study of solid oxide fuel cell materials," Energy Environ. Sci. **7**, 306–310 (2014).
[16]J. Sylvia, J. Janni, J. Klein, and K. Spencer, "Surface-enhanced Raman detection of 2,4-dinitrotoluene impurity vapor as a marker to locate landmines," Anal. Chem. **72**, 5834–5840 (2000).
[17]D. L. Jeanmaire and R. P. V. Duyne, "Surface Raman spectroelectrochemistry," J. Electroanal. Chem. Interf. Electrochem. **84**, 1–20 (1977).
[18]D. Cialla, A. März, R. Böhme, F. Theil, K. Weber, M. Schmitt, and J. Popp, "Surface-enhanced Raman spectroscopy (SERS): Progress and trends," Anal. Bioanal. Chem. **403**, 27–54 (2012).
[19]R. J. Nemanich, C. C. Tsai, and G. A. N. Connell, "Interference-enhanced Raman scattering of very thin titanium and titanium oxide films," Phys. Rev. Lett. **44**, 273–276 (1980).
[20]I. H. Abidi, A. A. Cagang, A. Tyagi, M. A. Riaz, R. Wu, Q. Sun, and Z. Luo, "Oxidized nitinol substrate for interference enhanced Raman scattering of monolayer graphene," RSC Adv. **6**, 7093–7100 (2016).
[21]Y.-C. Lee, E.-Y. Wang, Y.-L. Liu, and H.-L. Chen, "Using metal-less structures to enhance the Raman signals of graphene by 100-fold while maintaining the band-to-band ratio and peak positions precisely," Chem. Mater. **27**, 876–884 (2015).
[22]T. Ciuk, A. Kozlowski, P. P. Michalowski, W. Kaszub, M. Kozubal, Z. Rekuc, J. Podgorski, B. Stanczyk, K. Przyborowska, I. Jozwik, A. Kowalik, and P. Kaminski, "Thermally activated double-carrier transport in epitaxial graphene on vanadium-compensated 6H-SiC as revealed by Hall effect measurements," Carbon **139**, 776–781 (2018).
[23]T. Ciuk, B. Stanczyk, K. Przyborowska, D. Czolak, A. Dobrowolski, J. Jagiello, W. Kaszub, M. Kozubal, R. Kozlowski, and P. Kaminski, "High-temperature Hall effect sensor based on epitaxial graphene on high-purity semiinsulating 4H-SiC," IEEE Trans. Electron Devices **66**, 3134–3138 (2019).
[24]L. Vančo, M. Kotlár, M. Kadlečíková, V. Vretenár, M. Vojs, and J. Kováč, Jr., "Interference-enhanced Raman scattering in SiO_2/Si structures related to reflectance," J. Raman Spectrosc. **50**, 1502–1509 (2019).
[25]T. Ciuk and W. Strupinski, "Statistics of epitaxial graphene for Hall effect sensors," Carbon **93**, 1042–1049 (2015).
[26]T. Ciuk, P. Caban, and W. Strupinski, "Charge carrier concentration and offset voltage in quasi-free-standing monolayer chemical vapor deposition graphene on SiC," Carbon **101**, 431–438 (2016).
[27]M. J. Szary, S. El-Ahmar, and T. Ciuk, "The impact of partial H intercalation on the quasi-free-standing properties of graphene on SiC(0001)," Appl. Surf. Sci. **541**, 148668 (2021).
[28]W. Strupinski, K. Grodecki, A. Wysmolek, R. Stepniewski, T. Szkopek, P. E. Gaskell, A. Gruneis, D. Haberer, R. Bozek, J. Krupka, and J. M. Baranowski, "Graphene epitaxy by chemical vapor deposition on SiC," Nano Lett. **11**, 1786–1791 (2011).
[29]E. Schilirò, R. L. Nigro, F. Roccaforte, I. Deretzis, A. L. Magna, A. Armano, S. Agnello, B. Pecz, I. G. Ivanov, R. Yakimova, and F. Giannazzo, "Seed-layer-free atomic layer deposition of highly uniform Al_2O_3 thin films onto monolayer epitaxial graphene on silicon carbide," Adv. Mater. Interfaces **6**, 1900097 (2019).
[30]E. Schilirò, R. L. Nigro, S. Panasci, F. Gelardi, S. Agnello, R. Yakimova, F. Roccaforte, and F. Giannazzo, "Aluminum oxide nucleation in the early stages of atomic layer deposition on epitaxial graphene," Carbon **169**, 172–181 (2020).
[31]A. Dobrowolski, J. Jagiełło, D. Czolak, and T. Ciuk, "Determining the number of graphene layers based on Raman response of the SiC substrate," Physica E **134**, 114853 (2021).